

Deep Defects in $\text{Cu}_2\text{ZnSn}(\text{S,Se})_4$ Solar Cells with Varying Se Content

S. Levchenko,^{1,*} J. Just,¹ A. Redinger,¹ G. Larramona,² S. Bourdais,² G. Dennler,² A. Jacob,² and T. Unold^{1,†}

¹*Helmholtz-Zentrum Berlin für Materialien und Energie (HZB),*

Hahn-Meitner-Platz 1, D-14109 Berlin, Germany

²*IMRA Europe S.A.S., 220 rue Albert Caquot, 06904 Sophia Antipolis, France*

(Received 20 April 2015; revised manuscript received 12 November 2015; published 16 February 2016)

Electronic defects in $\text{Cu}_2\text{ZnSn}(\text{Se}_x\text{S}_{1-x})_4$ ($x = 0, 0.4, 0.6,$ and 1) kesterite solar cells are studied by temperature-dependent admittance spectroscopy and photoluminescence studies. Using admittance spectroscopy, we find that the substitution of sulfur by selenium decreases the depth of a dominant acceptor level from 0.29 to 0.12 eV. In addition, a deep-acceptor defect at about 0.5 eV above the valence band is found for the $x = 0.4$ – 1 devices. A shallow transition level with an energy of 0.14–0.09 eV is deduced from the thermal quenching of the photoluminescence yield, which we attribute to a donor level.

DOI: 10.1103/PhysRevApplied.5.024004

I. INTRODUCTION

Kesterite $\text{Cu}_2\text{ZnSn}(\text{Se}_x\text{S}_{1-x})_4$ (CZTSSe) absorber layers have been successfully implemented in solar cells with demonstrated conversion efficiencies of up to 12.6% [1]. Despite considerable research efforts, there are many open questions with regard to bulk and interface defect properties in kesterite materials and devices. For example, it is unclear what is the ultimate cause for the commonly observed low open-circuit voltage in these devices when compared to the theoretical limit [1–5]. In general, the open-circuit voltage deficiency increases with band gap for $\text{Cu}_2\text{ZnSn}(\text{S,Se})_4$ devices of varying Se content or for $\text{Cu}_2\text{Zn}(\text{Sn,Ge})(\text{S,Se})_4$ with varying Ge content [3,4]. For the higher-band-gap materials, a cliff in the conduction band with respect to CdS has been found experimentally, which would also support interface recombination [6]. This view is supported by the fact that, in most cases, the open-circuit extrapolation to zero kelvin falls short of the band-gap value [2]. However, more detailed analysis has shown that bulk recombination in combination with potential fluctuations and/or band tailing can also explain large voltage deficits in kesterite devices [3,4]. Experimental defect studies for kesterite solar cells have been rather limited so far, and no clear picture regarding the point-defect transition levels in kesterite materials has evolved. Most defect studies were based on characterizations by either photoluminescence [7–10] or by admittance spectroscopy [11–13] and often involved either sulfur compounds only, or a limited range of sulfur-to-selenium ratios, samples with varying cation ratios [9], or single-crystal

samples [14], which makes generalized conclusions difficult for polycrystalline thin films.

Experimentally, a clear correlation between the device efficiency and the cation ratios in the samples has been found by many groups, with the maximum efficiency generally obtained for slightly Cu-poor $[\text{Cu}]/([\text{Zn}] + [\text{Sn}]) \approx 0.85$ and slightly Zn-rich composition $\text{Zn}:\text{Sn} \approx 1.1$, although the reason for this phenomenon is not yet clear [15]. Also, the best devices have not been found for the pure S- or Se-containing compounds but rather for sulfoselenide composition, which also has not been explained to date. Defect studies, thus, are most useful when exploring these composition ratios and shed light on the effect of sulfur-selenium substitution on the defect properties of these compounds.

In this paper, we report a comprehensive analysis of the point-defect transition energies by admittance, photoluminescence, and temperature-dependent current-voltage (I – VT) analysis on a set of $\text{Cu}_2\text{ZnSn}(\text{Se}_x\text{S}_{1-x})_4$ devices ranging in composition from $x = 0$ to $x = 1$. All the different experimental methods are applied to identical devices. Please note that 60% selenium corresponds to a band gap of about 1.15 eV, which is in the range of the best devices reported by the IBM group.

II. EXPERIMENTAL DETAILS

The kesterite $\text{Cu}_2\text{ZnSn}(\text{Se}_x\text{S}_{1-x})_4$ absorbers ($x = 0, 0.4, 0.6$) are prepared with a nonvacuum and environmentally friendly preparation method reported recently [16,17]. This process consists of the following steps: synthesis of a Cu-Zn-Sn-S colloidal solution, redispersion of the colloids in a mixture of water (90%) and ethanol (10%), spray deposition on Mo-coated glass substrates, and, finally, a two-step annealing of the samples in N_2 and H_2S gases for the pure sulfide devices ($x = 0$) [16] or a two-step annealing in N_2 and a Se-containing atmosphere for the sulfide-selenide devices ($x = 0.4, 0.6$) [17]. The devices are finished by

*Corresponding author.

sergiu.levchenko@helmholtz-berlin.de

†Corresponding author.

unold@helmholtz-berlin.de

adding a CdS buffer and *i*-ZnO/ITO window layers. So far, cell efficiencies up to 10.8% have been achieved by this method [17]. In the present study, the solar-cell efficiencies of the $x = 0, 0.4, 0.6$ devices are 4.0%, 5.0%, and 6.6%, respectively. In addition, a CZTSe sample containing only selenium as chalcogen ($x = 1$) is prepared by selenization of a magnetron-sputtered precursor stack Mo/Cu/Sn/Zn/Cu deposited on soda-lime glass. The selenization is performed using Se pellets in a sealed quartz box with a maximum temperature of $T = 480^\circ\text{C}$ and duration of 20 min. Solar-cell devices are completed by chemical-bath deposition of CdS and magnetron sputtering of an *i*-ZnO- and Al-doped ZnO window. More detailed information about CZTSe cell preparation can be found in the Supplemental Material [18].

The cation ratios of the absorber layers are measured by X-ray fluorescence and show $[\text{Cu}]/([\text{Zn}] + [\text{Sn}]) \approx 0.88, 0.93, 0.86, 0.88$ and $\text{Zn}:\text{Sn} \approx 1.14, 1.26, 1.17, 1.09$ for the $x = 0, 0.4, 0.6, 1$ devices, respectively. All devices are slightly Cu poor and Zn rich within a range that normally leads to the best devices reported in the literature. The $[\text{Cu}]/([\text{Zn}] + [\text{Sn}])$ cation ratio for all devices is almost identical within the measurement error, which we estimate at ± 0.03 . The $x = 0$ and $x = 0.6$ samples also have identical Zn:Sn ratios, with a slightly larger and slightly smaller value for the $x = 0.4$ and $x = 1$ devices, respectively. However, since Zn excess is found to lead to a segregation of the ZnS secondary phase [19], we do not expect this small variation in Zn excess to affect our results.

For the different S/Se compositions, several samples are produced, such that at least 16 solar cells are available for each chalcogen composition. All of these devices are characterized by I - V T measurements and external quantum efficiency (EQE), and a smaller number is selected for the more detailed admittance and photoluminescence analysis. Although in this paper only data pertaining to one device for each composition are reported, the results obtained for different solar cells are found to be consistent. For CZTS ($x = 0$), a solar cell prepared by coevaporation [20] has been studied by admittance for comparison, yielding a general behavior and activation energy consistent with the solution-processed pure sulfur sample reported here.

Admittance measurements are performed with frequencies ranging from 100 Hz to 1 MHz with a 20-mV ac voltage using a HP 4284 LCR meter operated in R (resistance)- X (reactance) mode in the dark and at 0-V bias. Capacitance voltage profiling on the selected samples yields charge densities of $3 \times 10^{16}, 10^{17}, 4 \times 10^{16},$ and 10^{16} cm^{-3} at 1 kHz for the $x = 0, 0.4, 0.6,$ and 1 devices, respectively. I - V device characteristics are recorded using a Keithley 238 source measure unit. EQE measurements are performed using a halogen lamp dispersed by a 1/4-m monochromator and chopped at 90 Hz in conjunction with a low-noise current-voltage preamplifier and lock-in amplifier. Photoluminescence measurements are performed using

a 660-nm diode laser and a thermoelectrically cooled InGaAs diode array coupled to a 1/4-m grating monochromator. The excitation power intensity is adjusted with a set of neutral density filters. Temperature-dependent measurements are carried out in a closed-cycle helium cryostat where the sample temperature is measured with a silicon diode on top of an identical sample.

III. RESULTS AND DISCUSSION

In Fig. 1(a), we show the temperature-dependent complex impedance (Z) of the $x = 0.4$ device. Similar sets of $Z(f, T)$ curves are obtained for the $x = 0$ and $x = 0.6$ devices. In order to analyze $Z(f, T)$, we apply an equivalent circuit model which includes a capacitor (C_p) and a resistor (R_p) in parallel, plus a series resistance element (r) [21]. Using the series resistance r extracted from the real part of Z in the limit of high frequencies, the CZTSSe capacitance (C) can be derived from the real and imaginary parts of $Z(f, T)$. Note that this procedure removes the parasitic effects of series resistance from the impedance signal. $C(f, T)$ data for the $x = 1, 0.6, 0.4,$ and 0 devices are shown in Figs. 1(b)–1(d), and 1(e), respectively. Below 100 K, the capacitance curves weakly depend on the frequency, with an asymptotic value of about 3 to 6 nF cm⁻² (depending on the absorber thickness) at the lowest temperatures, which can be attributed to the geometrical capacitance value using static dielectric constants ϵ of 7.1, 8.3, 8.8, and 8.9 for the $x = 0, 0.4, 0.6,$ and 1 devices, respectively, which are derived from $C = \epsilon/d$, where d is the absorber-layer thickness measured from SEM cross sections. We point out that the determined dielectric constants ϵ agree well with those reported previously [11].

For higher temperatures, two steplike features are found in the temperature-dependent capacitance for the sulfoselenide devices, while only one capacitance step is observed for the $x = 0$ device. The activation energies E_A and attempt frequencies ξ of these capacitance steps can be obtained from an Arrhenius plot of the inflection points of the capacitance-vs-temperature plots [maxima of $-fdC(f)/df$] as shown in Fig. 1(f) and are defined as

$$\omega_0 = 2\pi f_0 = N_V v_{\text{th}} \sigma_p e^{-E_A/kT} = 2\xi_0 T^2 e^{-E_A/kT}, \quad (1)$$

where N_V is the effective density of states in the valence band, v_{th} is the thermal carrier velocity, and σ_p is the capture cross section for holes.

For the capacitance steps of the $x = 0.4, 0.6,$ and 1 devices, we find activation energies $E_{A1}^{\text{AS}} = 0.17, 0.13,$ and 0.12 eV, $E_{A2}^{\text{AS}} = 0.53, 0.50,$ and 0.48 eV, respectively [see Fig. 1(f)]. The thermal-emission prefactor ξ_{A1}^{AS} is found to be $5 \times 10^4, 2 \times 10^5,$ and $4 \times 10^4 \text{ s}^{-1} \text{ K}^{-2}$, and ξ_{A2}^{AS} is $10^8, 10^9,$ and $7 \times 10^8 \text{ s}^{-1} \text{ K}^{-2}$ for the $x = 0.4, 0.6,$ and 1 devices, respectively. For the $x = 0$ device, we find an

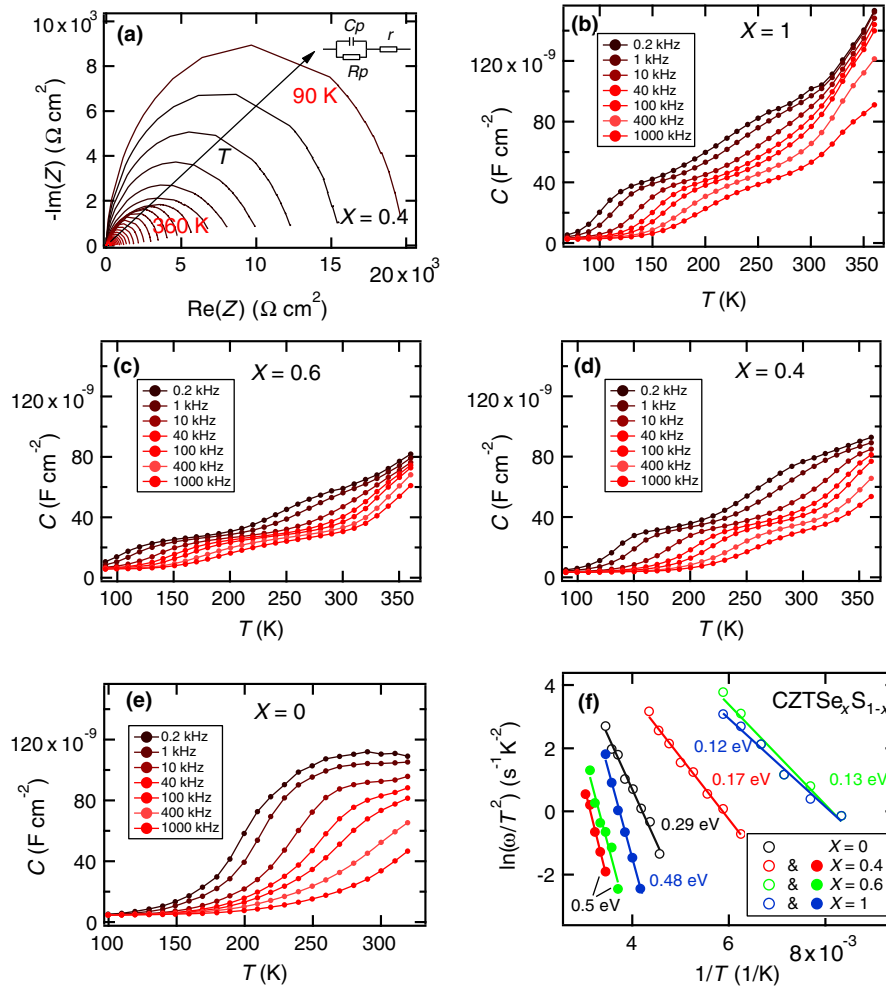


FIG. 1. (a) Nyquist plots of Z imaginary part, $\text{Im}(Z)$, versus Z real part, $\text{Re}(Z)$, of a $\text{Cu}_2\text{ZnSn}(\text{Se}_x\text{S}_{1-x})_4$ ($x = 0.4$) device. (b) $C(f, T)$ of a $\text{Cu}_2\text{ZnSn}(\text{Se}_x\text{S}_{1-x})_4$ ($x = 1$) device. (c) $C(f, T)$ of a $\text{Cu}_2\text{ZnSn}(\text{Se}_x\text{S}_{1-x})_4$ ($x = 0.6$) device. (d) $C(f, T)$ of a $\text{Cu}_2\text{ZnSn}(\text{Se}_x\text{S}_{1-x})_4$ ($x = 0.4$) device. (e) $C(f, T)$ of a $\text{Cu}_2\text{ZnSn}(\text{Se}_x\text{S}_{1-x})_4$ ($x = 0$) device. (f) Arrhenius plot of the inflection frequency of $\text{Cu}_2\text{ZnSn}(\text{Se}_x\text{S}_{1-x})_4$ ($x = 0, 0.4, 0.6, 1$) device; the fitted activation energies are indicated.

activation energy of 0.29 eV and a prefactor value of $7 \times 10^5 \text{ s}^{-1} \text{ K}^{-2}$ [see Fig. 1(f)]. The activation energies of the low-temperature capacitance step (0.12–0.29 eV) are in good agreement with recent admittance spectroscopy studies on hydrazine-processed CZTSSe devices, where a decrease in the defect activation energy with increasing x was also observed [11]. Similar values have also been reported for CZTSe/CdS and CZTS_{0.25}Se_{0.75}/CdS monograin heterojunctions, where activation energies of 0.09–0.1 and 0.075 eV were determined by temperature-dependent admittance spectroscopy (AS) [13]. In contrast to our results, several studies on CZTS have reported lower activation energies from AS measurements between 0.045 and 0.16 eV [22–24]. However we note that some of these results were obtained on very-low-efficiency devices [22,23] and with possibly incomplete equivalent circuit-model analysis [22,24].

The deep defect observed at 0.5–0.53 eV can indicate a limiting bulk recombination process in kesterite devices,

considering that the thermal-emission energy is located almost at midgap in the $x = 0.4$ –1 devices. The fact that this defect transition is not seen for the $x = 0$ device is likely due to the fact that the energetically more shallow defect transition in this device dominates the capacitance response: the capacitance step for this device amounts to a $\Delta C = 100 \text{ nF}$ which is much larger than the low-temperature capacitance step observed in the other three devices.

Comparing the observed defect activation energies with the defect transition levels and formation energies calculated by density-functional theory (DFT) [25], we believe that the more shallow defect is most likely associated with the Cu_{Zn} antisite defect. Among the possible acceptor defects in CZTSSe, Cu_{Zn} and V_{Cu} have been found to exhibit by far the lowest formation energies using both local functionals [25] and hybrid methods in DFT [26]. For the copper vacancy, both calculations find a very shallow 0 to $-$ transition energy between 16 [25] and 70 meV [26], which is much smaller than the observed

activation energies. On the other hand, the calculations show the Cu_{Zn} transition level to be deeper with 0 to $-$ energies for CZTS of 220 [26] to 150 meV [25] and 110 meV for CZTSe [25]. Although the formation of this defect may seem unlikely given the Cu-poor and Zn-rich growth conditions, the calculations show that also for these conditions, the formation energy can be sufficiently low to make Cu_{Zn} the dominant acceptor level. The experimentally observed activation energy of 120 meV for CZTSe becoming deeper for increasing sulfur content with a final value of 290 meV for the CZTS devices supports the theoretical findings that the ionization energy deepens with increasing sulfur content. Please note that the formation energy of the Zn_{Sn} antisite acceptor defect has also been found to be relatively low in an earlier calculation [27], which would predict also large concentrations for this defect, especially when taking into account vibrational free-energy changes associated with this defect [28]. However, the formation energy for this defect in later calculations has been found considerably larger [25,26], such that we do not consider an assignment of our experimentally determined acceptor levels to this defect.

With respect to the deep level at about 500 meV above the valance-band maximum (VBM), possible defects are Cu_{Sn} antisites or V_{Sn} vacancies, which have been found to exhibit deep transition levels in DFT calculations [25,26]. We note that these defects will be promoted by Sn loss, which, on the other hand, has been observed to be a major experimental bottleneck related to kesterite thin-film synthesis [29]. Indeed, in a recently published study [17] reporting the optimization of CZTSSe devices with $x = 0.6$, we show that the increase of the Sn content in the synthesis process leads to a reduction of the midgap defects reported in this study.

Previous studies have found a thermally activated series resistance in I - VT measurements, which has been attributed to either bulk resistivity [11] or a back contact barrier [30] and also has been associated with the temperature-dependent capacitance response evaluated in admittance measurements [12,31]. We measure the I - VT characteristics on our devices (see Fig. S1 in the Supplemental Material [18]) and find a thermally activated series resistance evaluated under forward bias (see Fig. 2). Assuming thermionic emission across a back contact barrier, the series resistance can be described by $R_s(T) = R_0 + k/(qA^*T) \exp(\Phi_B/kT)$, where A^* is the effective Richardson constant, k is the Boltzmann constant, and Φ_B is the barrier height (for the derivation, see the Supplemental Material [18]). We obtain barrier heights Φ_B of 0.03, 0.25, 0.16, and 0.09 eV for the $x = 0, 0.4, 0.6,$ and 1 devices, respectively (see Fig. 2). The barrier heights for the $x = 0$ and 0.4 devices are clearly different from the AS-derived values for the activation energies. Although the $\Phi_B \approx 0.16$ eV of the $x = 0.6$ device is close to the value of 0.13 eV determined from AS measurements at

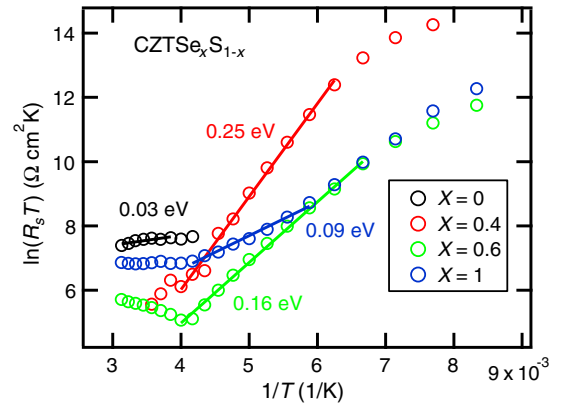


FIG. 2. Solar-cell-series resistance R_s of $\text{Cu}_2\text{ZnSn}(\text{Se}_x\text{S}_{1-x})_4$ ($x = 0, 0.4, 0.6, 1$) devices; the fitted activation energies are indicated.

120–170 K [Fig. 1(e)], we note that for several additional samples containing 60% selenium, activation energies of 120–150 meV are measured by AS, while the barrier height inferred from I - VT measurements is of order 200 meV. Thus, we conclude that the activated behavior of the dc-series resistance is not related to the admittance response for our devices but may be related to the presence of a secondary barrier in the CZTSSe device. Although the I - VT -determined-series resistance is used in the literature to correct the admittance response, we point out that these values are determined under forward bias, whereas the admittance is measured without external bias, such that the ac-series resistance at 0 V and the dc-series resistance at forward bias do not have to coincide. For our devices, we clearly see that the AS-series resistance does not strongly depend on the temperature, while the I - VT -series resistance shows an activated character (see Fig. S2 in the Supplemental Material [18]).

The results of the temperature- and excitation-dependent photoluminescence (PL) of the CZTSSe devices are presented in Fig. 3. For all compositions, we find a broad emission PL band (FWHM = 0.15, 0.13, 0.11, and 0.09 eV for $x = 0, 0.4, 0.6,$ and 1), the maximum of which gradually shifts to the low-energy side with increasing selenium content [see Fig. 3(a)] and shows a strong blueshift with respect to the excitation power [β factor of approximately 12–17 meV/decade at 20 K; see inset of Fig. 3(a)]. Another interesting trend of the CZTSSe PL properties is the temperature dependence: The emission PL maximum redshifts by increasing the temperature up to approximately 180 K [see Figs. 3(c) and 3(d)]. These temperature and excitation characteristics have also been observed in ternary chalcopyrite materials [32,33] and have been attributed to the presence of spatial potential fluctuations caused by large densities of donor- and acceptor-type defects [34,35]. In this case, a quasi-donor-acceptor-pair (QDAP) recombination process instead of a donor-acceptor pair takes place

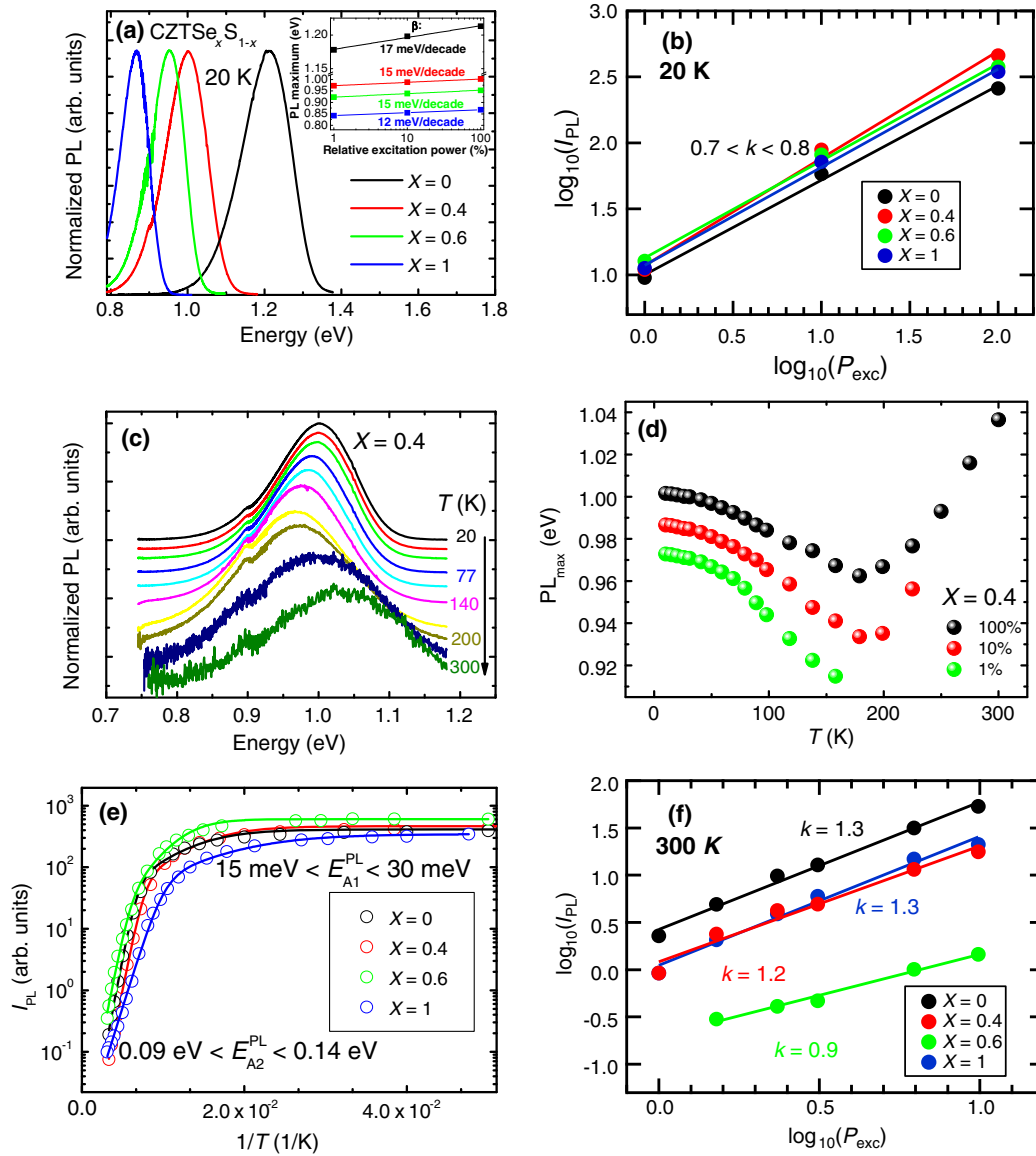


FIG. 3. (a) PL spectra for $\text{Cu}_2\text{ZnSn}(\text{Se}_x\text{S}_{1-x})_4$ ($x = 0, 0.4, 0.6, 1$) devices at 20 K at 100% relative excitation power. Inset: PL maximum as a function of the relative excitation power. (b) Integrated PL intensity as a function of the excitation power of $\text{Cu}_2\text{ZnSn}(\text{Se}_x\text{S}_{1-x})_4$ ($x = 0, 0.4, 0.6, 1$) devices at 20 K. The straight lines are linear fits to $I_{\text{PL}} = (P_{\text{exc}})^k$. (c) PL spectra as a function of T for a $\text{Cu}_2\text{ZnSn}(\text{Se}_x\text{S}_{1-x})_4$ ($x = 0.4$) device. (d) PL maximum as a function of T for a $\text{Cu}_2\text{ZnSn}(\text{Se}_x\text{S}_{1-x})_4$ ($x = 0.4$) device at different excitation levels. (e) Integrated PL intensity as a function of T for a $\text{Cu}_2\text{ZnSn}(\text{Se}_x\text{S}_{1-x})_4$ ($x = 0, 0.4, 0.6, 1$) devices (the fitted activation energy is indicated). (f) Integrated PL intensity as a function of the excitation power of $\text{Cu}_2\text{ZnSn}(\text{Se}_x\text{S}_{1-x})_4$ ($x = 0, 0.4, 0.6, 1$) devices at 300 K.

[32,34]. We also attribute the main PL transitions in our kesterite samples to a QDAP recombination type.

As shown in Fig. 4, the PL transition energy for QDAP transitions is given [32,34] by $E_{\text{QDAP}} \approx E_g - (E_A + E_D) - 2\Gamma$, where E_g is the band-gap energy, E_D and E_A are the donor and acceptor ionization energies, respectively, and Γ is the average potential well depth. In the original references [32,34] introducing the QDAP model, the donor-acceptor pair Coulomb interaction ($E_Q = e^2/4\pi\epsilon\epsilon_0 r$, where r is the donor-acceptor pair separation, e is the electric charge of the electron, and

ϵ_0 is the dielectric constant of the vacuum) was omitted in the E_{QDAP} formulas and assumed to be negligible in comparison to the Γ term. From the excitation-dependent PL measurements, we obtain shifts of the PL maximum by 24–34 meV, over 2 orders of excitation intensity, which, in the following, we compare with a possible shift induced by the Coulomb term. In the theory of Zacks and Halperin [36] describing DAP recombination, the maximum value for the Coulomb term is expressed by $E_Q^{\text{max}} = e^2/4\pi\epsilon\epsilon_0(2r_B) = 13.6m^*/\epsilon^2$, where r_B is the shallow impurity Bohr radius, and m^* is an effective mass at the impurity. By using

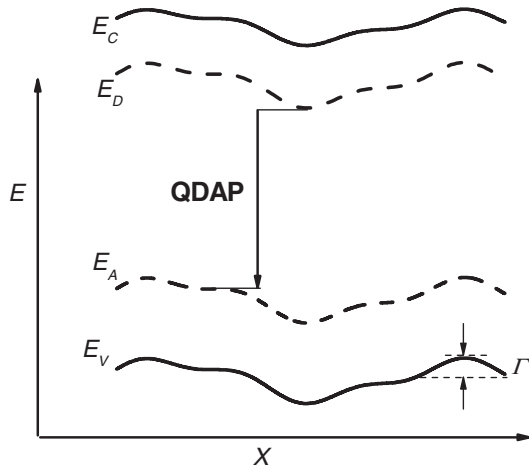


FIG. 4. A schematic representation for the QDAP transitions in the case of the presence of the potential fluctuations with an average depth of Γ . Here, we assume that E_V valence-band states, E_C conduction-band states, E_A acceptor level, and E_D donor level follow the variation of the potential fluctuation within the real space in CZTSSe.

theoretical values of the electron effective mass [37] as well as the static dielectric constant ϵ determined earlier, we estimate $E_Q^{\max} \approx 50$ and 14 meV for CZTS and CZTSe; see Fig. 5(a). However, as shown in Fig. 5(b), the contribution of the E_Q to E_{QDAP} depends on the excitation intensity range, and it is much smaller than the E_Q^{\max} values. The highest contribution of the E_Q is estimated to be 15 (4) meV with a rate of approximately 8 (2) meV/decade for CZTS (CZTSe). From these estimations, we can exclude the influence of the E_Q term for sulfoselenide devices, whereas in sulfur devices, it may partly contribute only for the highest excitation intensity values. It is also important to note that our calculations of the Coulomb term in the framework of the Zacks and Halperin [36] theory raise questions with regard to the validity of recent estimations of the donor-acceptor pair densities and distances in CZTS absorbers, where no Γ term was taken into account and where the rate for the PL maximum shift with

respect to the excitation intensity range measured was not considered [38].

The perturbation of the band states and the defect levels in semiconductors occurs due to compositional fluctuations and/or as a result of electrostatic potential fluctuations caused by a random distribution of charged defects. Here we consider that the parameter Γ in the QDAP model accounts for all of these possible contributions to the potential fluctuations. For the case of the compositional fluctuations, the gradual filling of the energy states within the band tails causes a PL blueshift with increasing excitation intensity at constant temperature [39,40]. In the case of a strong contribution from the charged defects, a shielding of the electrostatic potential by photogenerated carriers leads to a blueshift of the PL emission [32]. The observed redshift of the PL peak position up to approximately 180 K can be explained by a redistribution of carriers from localized defect states to the nearest deeper states before recombination [39]. In addition, the temperature dependence of the band gap contributes to the PL redshift [41].

The analysis of the integrated PL intensity (I_{PL}) shows a strong quenching of 3 orders of magnitude [Fig. 3(e)] with increasing temperature, which is well described by an expression with two activation energies [8],

$$I_{\text{PL}} = I_0 / [1 + \alpha_1 \exp(-E_{A1}^{\text{PL}}/kT) + \alpha_2 \exp(-E_{A2}^{\text{PL}}/kT)], \quad (2)$$

where I_0 is the intensity at the lowest temperature, and a_1 and a_2 are the rate parameters of the nonradiative process with activation energies of E_{A1}^{PL} (for $T < 100$ K) and E_{A2}^{PL} (for $T > 100$ K). For the $x = 0.4$ device, the determined activation energies are $E_{A1}^{\text{PL}} \approx 25$ meV and $E_{A2}^{\text{PL}} \approx 130$ meV [see Fig. 3(e)]. Very similar E_{A2}^{PL} values are obtained for all three sulfur-selenium devices (see Table I), indicating that this defect activation energy does not change with the Se content. Since we observe neither a blueshift of the PL with temperature nor changes in the PL peak excitation intensity

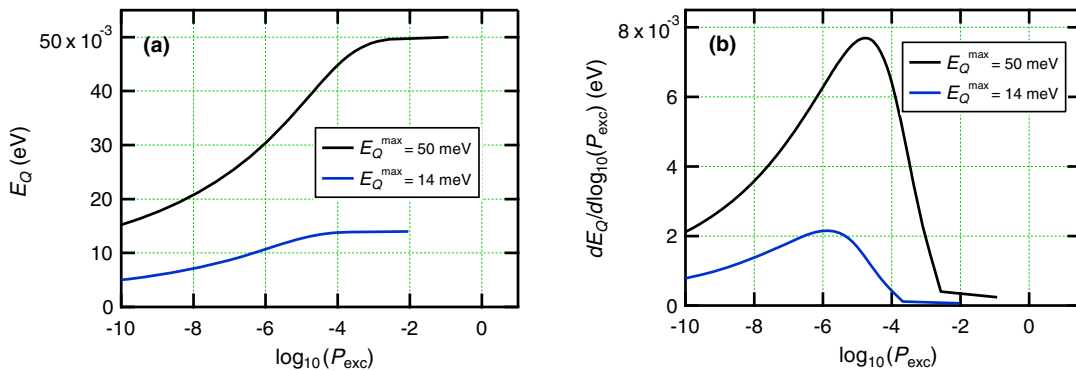


FIG. 5. (a) Calculated DAP emission shift due to Coulomb interaction [36] as a function of the excitation power for CZTS ($E_Q^{\max} = 50$ meV) and CZTSe ($E_Q^{\max} = 14$ meV). (b) First derivative, $dE_Q/d\log_{10}(P_{\text{exc}})$, of the DAP recombination emission showing the rate of this shift as a function of the excitation power.

TABLE I. Summary of data of the band diagram and defect states for CZTSSe devices with different Se content ($x = 0, 0.4, 0.6, 1$).

Method	Parameter	Assignment	$x = 0$	$x = 0.4$	$x = 0.6$	$x = 1$
EQE	Band gap	E_g (eV) ^a	1.5	1.30	1.15	1.00
DFT	VBM	VBM (eV) ^b	0	0.06	0.09	0.15
DFT	CBM	CBM (eV) ^b	1.5	1.36	1.29	1.15
PL	E_{A1}^{PL}	Γ (eV)	0.022	0.025	0.030	0.015
PL	E_{A2}^{PL}	$E_D - E_C$ (eV)	0.14	0.13	0.14	0.09
AS	E_{A2}^{AS}	$E_V - E_{A2}$ (eV)	...	0.53	0.50	0.48
AS	E_{A1}^{AS}	$E_V - E_{A1}$ (eV)	0.29	0.17	0.13	0.12
PL	$E_{A3}^{\text{PL}} = E_g - E_{l(\text{PL peak})}$	$E_V - E_{A3}$ (eV)	0.23	0.26	0.14	0.08
I - V T	E_A^{I-VT}	Φ_B (R_s dark) (eV) ^c	0.03	0.25	0.16	0.09
AS	Dielectric constant	ϵ	7.1	8.3	8.8	8.9

^aAt 300 K.^bRef. [42].^cNot related to defects in bulk CZTSSe.

dependence for $T < 180$ K, we do not assign E_{A1}^{PL} to the shallower level involved in QDAP recombination. Rather, we attribute E_{A1}^{PL} to the average valley depth from which carriers may be thermally emitted and as a free carrier may recombine nonradiatively.

On the other hand, E_{A2}^{PL} can be assigned either to the donor energy E_D or acceptor energy E_A , as the PL peak maximum significantly blueshifts [see Fig. 3(c)] when the temperature rises from 180 to 300 K, with the PL peak excitation intensity dependence disappearing for $T > 220$ K. Because CZTSSe absorbers are p type, we attribute E_{A2}^{PL} to a donor level since a conduction-band-to-acceptor transition is more probable [43]. According to first-principles DFT calculations, shallow donor-related transitions are expected for Zn_{Cu} and Sn_{Cu} antisites, as well as for Cu_i , Zn_i , and Sn_i interstitials [26,27]. Considering the formation energies for these defects and the Cu-poor and Zn-rich growth conditions, we conclude that E_{A2}^{PL} is most likely associated with the Zn_{Cu} donor defect.

Taking into account the band-gap values E_g estimated from the derivative of EQE curves (not shown here) and PL peak energy, we associate the room-temperature PL emission to a free-to-bound transition, from the conduction band to an acceptor level located at $E_{A3}^{\text{PL}} = 0.08$ – 0.26 eV above the valence-band maximum (see Table I). We note that k , the exponent of the power law of the luminescence intensity vs excitation power, of the room temperature PL is found to be 0.9–1.3 [see Fig. 3(f)], while the low-temperature k is 0.7–0.8 for CZTSSe [see Fig. 3(b)]. Although $k > 1$ is usually attributed to band-to-band-type transitions [44], it has been shown that this is not a general behavior [45] and values $k > 1$ can be observed for defect-related transitions, too [45,46]. As detailed in the Appendix, we show that in the case where neutral donors participate in the dynamics of defect state transitions, the k of the free-to-acceptor transition can be up to twice as large as the k of the DAP transition, which, as a rough estimation, can be related to

our measured value of 0.7–0.8 [see Fig. 3(b)]. From the point of view of the transition energy, the room-temperature PL emission for the sulfoselenide devices is 260–140 meV below the E_g , which makes it likely that defects are involved in this PL transition. In the case of the CZTSSe sample, the difference between E_g and the PL band maximum is smaller and about 80 meV, such that a participation of band-to-band transitions in addition to free-to-bound transition cannot be excluded.

The defect-level energies obtained from AS and PL are summarized in a schematic defect diagram shown in Fig. 6. According to the first-principles calculations on the CZTSSe system, a substitution of S by Se atoms lowers the conduction-band minimum (CBM) by 0.35 eV, while the VBM shifts upwards by 0.15 eV [42]. There are only a few experimental studies available which deduce the CBM and VBM positions from ultraviolet photoemission and

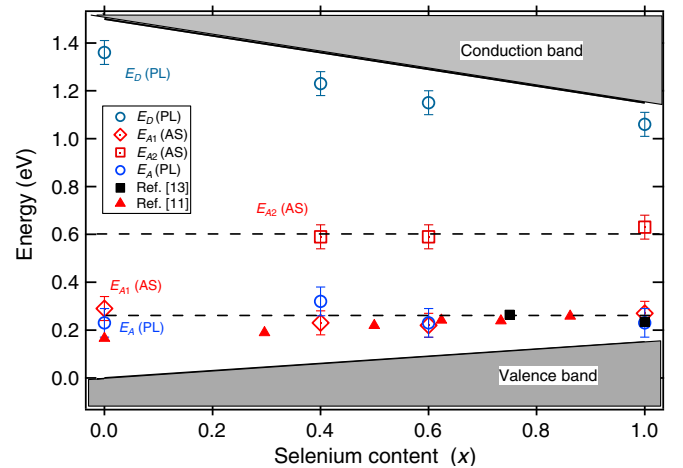


FIG. 6. A schematic defect band diagram of the defect levels for $\text{Cu}_2\text{ZnSn}(\text{Se}_x\text{S}_{1-x})_4$ ($x = 0, 0.4, 0.6, \text{ and } 1$) devices. Dashed lines are guides to the eye.

inverse photoemission [6,47]. The measurement uncertainty (which we estimate >100 meV) cumulated with the data scattering from the strongly-process-dependent interface properties, may turn quite consistent with the theoretical prediction, provided more experimental data are available. We will, therefore, resort to the theoretically predicted values. The resulting VBM and CBM dependences on x together with the measured band gap and the defect levels deduced from PL and admittance are plotted in Fig. 6. A good agreement between the shallow acceptor energies derived from the luminescence transition energy (E_{A3}^{PL}) and from admittance (E_{A1}^{AS}) is found, strengthening the present analysis of an acceptor defect-level energy E_A , tentatively attributed to the Cu_{Zn} antisite defect. Interestingly, when plotting the defect transition energies on this energy scale, the deep-acceptor defects remain at an approximately constant energy with respect to the vacuum level for different selenium contents, while the more shallow acceptor defects tend to become slightly deeper for increasing sulfur content. The shallow donor levels, on the other hand, follow the conduction band at an almost constant distance over the whole composition range. An almost constant energy position of deep defects with respect to the vacuum level has been previously predicted theoretically and verified experimentally for transition metal impurities in III–V and II–VI semiconductors [48,49] but later also observed for some intrinsic defects in $\text{Cu}(\text{In}, \text{Ga})(\text{S}, \text{Se})_2$ semiconductors [50]. From a device-performance perspective, the deep acceptors are expected to have the biggest impact on nonradiative recombination and should be minimized by appropriate sample preparation conditions, as demonstrated in a recent publications for $\text{Se} = 60\%$ devices [17]. The fact that the ionization energy of the more shallow acceptor level decreases with increasing selenium content is consistent with the empirical fact that the highest efficiencies so far have been achieved for devices with relatively high selenium content above 60%.

IV. CONCLUSIONS

In conclusion, we investigate the defect properties for $\text{Cu}_2\text{ZnSn}(\text{Se}_x\text{S}_{1-x})_4$ solar-cell devices fabricated by a colloidal spray method ($x = 0, 0.4, \text{ and } 0.6$) and by selenization of sputtered-metal precursors ($x = 1$). From temperature-dependent admittance measurements, we determine the activation energies of two capacitance steps, which we assign to two acceptor-type defect levels: a defect level with a thermal-emission energy 0.29–0.12 eV depending on the Se content and a deeper level of 0.5 eV close to midgap, which is detectable only in the sulfoselenide devices ($x = 0.4, 0.6, \text{ and } 1$). The defect transition energies deduced from temperature-dependent PL measurements are 0.13–0.09 eV, which we assign to a donor level.

ACKNOWLEDGMENTS

The authors thank Joachim Klaer and Lars Steinkopf for the solar cell preparations. The authors would like to thank Steffen Kretschmar for the PL measurements and valuable discussions. A. R. acknowledges financial support from the Fonds national de la recherche, Project No. 7842175.

APPENDIX POWER-LAW COEFFICIENTS OF DONOR-ACCEPTOR-PAIR AND FREE-TO-ACCEPTOR TRANSITIONS

Here we follow the approach by Zubiaga *et al.* [45], which shows a procedure to evaluate power-law coefficients. For any type of PL transition, a power-law coefficient is expressed as [44,45]

$$k_i = \frac{d \ln I_{\text{PL}}^i}{d \ln P_{\text{exc}}} = \frac{P_{\text{exc}}}{I_{\text{PL}}^i} \frac{d I_{\text{PL}}^i}{d P_{\text{exc}}}, \quad (\text{A1})$$

where i denotes type of recombination emission [free to acceptor (FA), DAP, excitonic, and band to band].

We consider here FA and DAP PL transitions, whose intensities are [44,45]

$$I_{\text{PL}}^{\text{FA}} \propto n N_{A0}, \quad (\text{A2a})$$

$$I_{\text{PL}}^{\text{DAP}} \propto N_{D0} N_{A0}, \quad (\text{A2b})$$

where n is the free-electron concentration, and N_{A0} and N_{D0} are the neutral acceptor and donor concentrations.

From Eqs. (A1) and (A2), the power-law coefficients for FA and DAP transitions are given by

$$k_{\text{FA}} = k_n + k_{A0}, \quad (\text{A3a})$$

$$k_{\text{DAP}} = k_{D0} + k_{A0}, \quad (\text{A3b})$$

where k_n is the power-law coefficient for the free-electron concentration, and k_{A0} and k_{D0} are the power-law coefficients for the neutral acceptor and donor concentrations, respectively.

By neglecting the donor-to-band transition for trapped electrons and ionization electrons from neutral donor by excitation laser from the rate equation for N_{D0} , we find that [45]

$$k_{D0} = k_n - \frac{1}{1 + \alpha} k_n - \frac{\alpha}{1 + \alpha} k_{A0} \quad (\text{A4})$$

with $\alpha = GN_{A0}/En$, where G is the rate probability for the DAP transition, and E is the rate probability for the electron trapping by the donor.

Assuming a nonzero value for α , we can rewrite Eq. (A4) as

$$k_n = \frac{1 + \alpha}{\alpha} k_{D0} + k_{A0}. \quad (\text{A5})$$

Finally, substituting Eq. (A5) into Eq. (A3a), we have

$$k_{\text{FA}} = \frac{1 + \alpha}{\alpha} k_{D0} + 2k_{A0} = \frac{1 - \alpha}{\alpha} k_{D0} + 2k_{\text{DAP}}. \quad (\text{A6})$$

For $\alpha \geq 1$, Eq. (A6) predicts $k_{\text{DAP}} + k_{A0} < k_{\text{FA}} < 2k_{\text{DAP}}$, while for $\alpha \ll 1$, we obtain $k_{\text{FA}} \approx \frac{1}{\alpha} k_{D0} + 2k_{\text{DAP}}$. From these estimations, we see that k_{FA} can approach values up to $2k_{\text{DAP}}$.

-
- [1] W. Wang, M. T. Winkler, O. Gunawan, T. Gokmen, T. K. Todorov, Y. Zhu, and D. B. Mitzi, Device characteristics of CZTSSe thin-film solar cells with 12.6% efficiency, *Adv. Energy Mater.* **4**, 1301465 (2014).
- [2] O. Gunawan, T. K. Todorov, and D. B. Mitzi, Loss mechanisms in hydrazine-processed CZTSSe solar cells, *Appl. Phys. Lett.* **97**, 233506 (2010).
- [3] T. Gokmen, O. Gunawan, T. K. Todorov, and D. B. Mitzi, Band tailing and efficiency limitation in kesterite solar cells, *Appl. Phys. Lett.* **103**, 103506 (2013).
- [4] C. J. Hages, N. J. Carter, R. Agrawal, and T. Unold, Generalized current-voltage analysis and efficiency limitations in non-ideal solar cells: Case of $\text{Cu}_2\text{ZnSn}(\text{Se}_x\text{S}_{1-x})_4$ and $\text{Cu}_2\text{Zn}(\text{Sn}_y\text{Ge}_{1-y})(\text{S}_x\text{Se}_{1-x})_4$, *J. Appl. Phys.* **115**, 234504 (2014).
- [5] A. Redinger and S. Siebentritt, in *Copper Zinc Tin Sulfide Based Thin-Film Solar Cells*, edited by K. Ito (Wiley, New York, 2015), Chap. 16.
- [6] M. Bär, B.-A. Schubert, B. Marsen, R. G. Wilks, S. Pookpanratana, M. Blum, S. Krause, T. Unold, W. Yang, L. Weinhardt, C. Heske, and H.-W. Schock, Cliff-like conduction band offset and KCN-induced recombination barrier enhancement at the CdS/ $\text{Cu}_2\text{ZnSnS}_4$ thin-film solar cell heterojunction, *Appl. Phys. Lett.* **99**, 222105 (2011).
- [7] M. Grossberg, J. Krustok, J. Raudoja, K. Timmo, M. Altosaar, and T. Raadik, Photoluminescence and Raman study of $\text{Cu}_2\text{ZnSn}(\text{Se}_x\text{S}_{1-x})_4$ monograins for photovoltaic applications, *Thin Solid Films* **519**, 7403 (2011).
- [8] F. Luckert, D. I. Hamilton, M. V. Yakushev, N. S. Beattie, G. Zoppi, M. Moynihan, I. Forbes, A. V. Karotki, A. V. Mudryi, M. Grossberg, J. Krustok, and R. W. Martin, Optical properties of high quality $\text{Cu}_2\text{ZnSnSe}_4$ thin films, *Appl. Phys. Lett.* **99**, 062104 (2011).
- [9] X. Lin, A. Ennaoui, S. Levchenko, T. Dittrich, J. Kavalakkatt, S. Kretzschmar, T. Unold, and M. Ch. Lux-Steiner, Defect study of $\text{Cu}_2\text{ZnSn}(\text{Se}_x\text{S}_{1-x})_4$ thin film absorbers using photoluminescence and modulated surface photovoltage spectroscopy, *Appl. Phys. Lett.* **106**, 013903 (2015).
- [10] K. Tanaka, Y. Miyamoto, H. Uchiki, K. Nakazawa, and H. Araki, Donor-acceptor pair recombination luminescence from $\text{Cu}_2\text{ZnSnS}_4$ bulk single crystals, *Phys. Status Solidi (a)* **203**, 2891 (2006).
- [11] O. Gunawan, T. Gokmen, C. W. Warren, J. D. Cohen, T. K. Todorov, D. A. R. Barkhouse, S. Bag, J. Tang, B. Shin, and D. B. Mitzi, Electronic properties of the $\text{Cu}_2\text{ZnSn}(\text{Se}, \text{S})_4$ absorber layer in solar cells as revealed by admittance spectroscopy and related methods, *Appl. Phys. Lett.* **100**, 253905 (2012).
- [12] T. P. Weiss, A. Redinger, J. Luckas, M. Mousel, and S. Siebentritt, Admittance spectroscopy in kesterite solar cells: Defect signal or circuit response, *Appl. Phys. Lett.* **102**, 202105 (2013).
- [13] E. Kask, M. Grossberg, R. Josepson, P. Salu, K. Timmo, and J. Krustok, Defect studies in $\text{Cu}_2\text{ZnSnSe}_4$ and $\text{Cu}_2\text{ZnSn}(\text{Se}_{0.75}\text{S}_{0.25})_4$ by admittance and photoluminescence spectroscopy, *Mater. Sci. Semicond. Process.* **16**, 992 (2013).
- [14] S. Levchenko, V. E. Tezlevan, E. Arushanov, S. Schorr, and T. Unold, Free-to-bound recombination in near stoichiometric $\text{Cu}_2\text{ZnSnS}_4$ single crystals, *Phys. Rev. B* **86**, 045206 (2012).
- [15] H. Katagiri, K. Jimbo, M. Tahara, H. Araki, and K. Oishi, The influence of the composition ratio on CZTS-based thin film solar cells, *Mater. Res. Soc. Symp. Proc.* **1165**, 1165-M04-01 (2009).
- [16] G. Larramona, S. Bourdais, A. Jacob, C. Choné, T. Muto, Y. Cuccaro, B. Delatouche, C. Moisan, D. Péré, and G. Dennler, Efficient $\text{Cu}_2\text{ZnSnS}_4$ solar cells spray coated from a hydro-alcoholic colloid synthesized by instantaneous reaction, *RCS Adv.* **4**, 14655 (2014).
- [17] G. Larramona, S. Levchenko, S. Bourdais, A. Jacob, C. Choné, B. Delatouche, C. Moisan, J. Just, T. Unold, and G. Dennler, Fine-tuning the Sn content in CZTSSe thin films to achieve 10.8% solar cell efficiency from a spray-deposited water-ethanol based colloidal inks, *Adv. Energy Mater.* **5**, 1501404, (2015).
- [18] See the Supplemental Material at <http://link.aps.org/supplemental/10.1103/PhysRevApplied.5.024004> for additional methods and results.
- [19] J. Just, D. Lützenkirchen-Hecht, R. Frahm, S. Schorr, and T. Unold, Determination of secondary phases in kesterite $\text{Cu}_2\text{ZnSnS}_4$ thin films by x-ray absorption near edge structure analysis, *Appl. Phys. Lett.* **99**, 262105 (2011).
- [20] B. A. Schubert, B. Marsen, S. Cinque, T. Unold, R. Klenk, S. Schorr, and H.-W. Schock, $\text{Cu}_2\text{ZnSnS}_4$ thin film solar cells by fast co-evaporation, *Prog. Photovoltaics* **19**, 93 (2011).
- [21] J. H. Scofield, Effects of series resistance and inductance on solar cell admittance measurements, *Sol. Energy Mater. Sol. Cells* **37**, 217 (1995).
- [22] E. Kask, T. Raadik, M. Grossberg, R. Josepson, and J. Krustok, Deep defects in $\text{Cu}_2\text{ZnSnS}_4$ monograin solar cell, *Energy Procedia* **10**, 261 (2011).
- [23] A. Fernandes, A. F. Sartori, P. M. P. Salomé, J. Malaquias, A. F. da Cunha, M. P. F. Graca, and J. C. Gonzalez, Admittance spectroscopy of $\text{Cu}_2\text{ZnSnS}_4$ based thin film solar cells, *Appl. Phys. Lett.* **100**, 233504 (2012).
- [24] L. Yin, G. Cheng, Y. Feng, Z. Li, C. Yang, and X. Xiao, Limitation factors for the performance of kesterite $\text{Cu}_2\text{ZnSnS}_4$ thin film solar cells studied by defect characterization, *RSC Adv.* **5**, 40369 (2015).
- [25] S. Chen, A. Walsh, X.-G. Gong, and S.-H. Wei, Classification of lattice defects in the kesterite $\text{Cu}_2\text{ZnSnS}_4$ and $\text{Cu}_2\text{ZnSnSe}_4$ earth-abundant solar cell absorbers, *Adv. Mater.* **25**, 1522 (2013).
- [26] D. Han, Y. Y. Sun, J. Bang, Y. Y. Zhang, H. B. Sun, X.-B. Li, and S. B. Zhang, Deep electron traps and origin of p -type

- conductivity in the earth-abundant solar-cell material $\text{Cu}_2\text{ZnSnS}_4$, *Phys. Rev. B* **87**, 155206 (2013).
- [27] S. Chen, J. H. Yang, X. G. Gong, A. Walsh, and S. H. Wei, Intrinsic point defects and complexes in the quaternary kesterite semiconductor $\text{Cu}_2\text{ZnSnS}_4$, *Phys. Rev. B* **81**, 245204 (2010).
- [28] V. Kosyak, N. B. Mortazavi Amiri, A. V. Postnikov, and M. A. Scarpulla, Model of native point defect equilibrium in $\text{Cu}_2\text{ZnSnS}_4$ and application to one-zone annealing, *J. Appl. Phys.* **114**, 124501 (2013).
- [29] A. Weber, R. Mainz, and H. W. Schock, On the Sn loss from thin films of the material system Cu-Zn-Sn-S in high vacuum, *J. Appl. Phys.* **107**, 013516 (2010).
- [30] K. Wang, O. Gunawan, T. K. Todorov, B. Shin, S. J. Chey, N. A. Bojarczuk, D. B. Mitzi, and S. Guha, Thermally evaporated $\text{Cu}_2\text{ZnSnS}_4$ solar cells, *Appl. Phys. Lett.* **97**, 143508 (2010).
- [31] T. Eisenbarth, T. Unold, R. Caballero, C. A. Kaufmann, and H.-W. Schock, Interpretation of admittance, capacitance-voltage, and current-voltage signatures in Cu(In, Ga)Se₂ thin film solar cells, *J. Appl. Phys.* **107**, 034509 (2010).
- [32] P. W. Yu, Radiative recombination in melt-grown, and Cd-implanted CuInSe₂, *J. Appl. Phys.* **47**, 677 (1976).
- [33] I. Dirnstorfer, Mt. Wagner, D. M. Hofman, M. D. Lampert, F. Karg, and B. K. Meyer, Characterization of CuIn(Ga)Se₂ thin films, *Phys. Status Solidi (a)* **168**, 163 (1998).
- [34] P. W. Yu, Excitation-dependent emission in Mg-, Be-, Cd-, and Zn-implanted GaAs, *J. Appl. Phys.* **48**, 5043 (1977).
- [35] B. I. Shklovskii and A. L. Efros, *Electronic Properties of Doped Semiconductors* (Springer, Berlin, 1984).
- [36] E. Zacks and A. Halperin, Dependence of the peak energy of the pair-photoluminescence band on excitation intensity, *Phys. Rev. B* **6**, 3072 (1972).
- [37] C. Persson, Electronic and optical properties of $\text{Cu}_2\text{ZnSnS}_4$ and $\text{Cu}_2\text{ZnSnSe}_4$, *J. Appl. Phys.* **107**, 053710 (2010).
- [38] T. Gershon, B. Shin, N. Bojarczuk, T. Gokmen, S. Lu, and S. Guha, Photoluminescence characterization of a high-efficiency $\text{Cu}_2\text{ZnSnS}_4$ device, *J. Appl. Phys.* **114**, 154905 (2013).
- [39] M. Oueslati, M. Zouaghi, M. E. Pistol, L. Samuelson, H. G. Grimmeiss, and M. Balkanski, Photoluminescence study of localization effects induced by the fluctuating random alloy potential in indirect band-gap $\text{GaAs}_{1-x}\text{P}_x$, *Phys. Rev. B* **32**, 8220 (1985).
- [40] I. A. Buyanova, W. M. Chen, G. Pozina, J. P. Bergman, B. Monemar, H. P. Xin, and C. W. Tu, Mechanism for low-temperature photoluminescence in GaNAs/GaAs structures grown by molecular-beam epitaxy, *Appl. Phys. Lett.* **75**, 501 (1999).
- [41] P. K. Sarswat and M. L. Free, A study of energy band gap versus temperature for $\text{Cu}_2\text{ZnSnS}_4$ thin films, *Physica (Amsterdam)* **407B**, 108 (2012).
- [42] S. Chen, A. Walsh, J.-H. Yang, X. G. Gong, L. Sun, P.-X. Yang, J.-H. Chu, and S.-H. Wei, Compositional dependence of structural and electronic properties of $\text{Cu}_2\text{ZnSn}(\text{S}, \text{Se})_4$ alloys for thin film solar cells, *Phys. Rev. B* **83**, 125201 (2011).
- [43] J. Krustok, J. H. Schon, H. Collan, M. Yakushev, J. Mudasson, and E. Bucher, Origin of the deep center photoluminescence in CuGaSe₂ and CuInS₂ crystals, *J. Appl. Phys.* **86**, 364 (1999).
- [44] T. Schmidt, K. Lischka, and W. Zulehner, Excitation-power dependence of the near-band-edge photoluminescence of semiconductors, *Phys. Rev. B* **45**, 8989 (1992).
- [45] A. Zubiaga, J. A. García, F. Plazaola, V. Muñoz-Sanjosé, and C. Martínez-Tomás, Near band edge recombination mechanisms in GaTe, *Phys. Rev. B* **68**, 245202 (2003).
- [46] Y. Gu, I. L. Kuskovsky, G. F. Neumark, X. Zhou, O. Maksimov, S. P. Guo, and M. C. Tamargo, Observation of free-to-acceptor-type photoluminescence in chlorine-doped Zn(Be)Se, *J. Lumin.* **104**, 77 (2003).
- [47] N. Terada, S. Yoshimoto, K. Chochi, T. Fukuyama, M. Mitsunaga, H. Tampo, H. Shibata, K. Matsubara, S. Niki, N. Sakai, T. Katou, and H. Sugimoto, Characterization of electronic structure of $\text{Cu}_2\text{ZnSn}(\text{S}_x\text{Se}_{1-x})_4$ absorber layer and CdS/ $\text{Cu}_2\text{ZnSn}(\text{S}_x\text{Se}_{1-x})_4$ interfaces by *in-situ* photoemission and inverse photoemission spectroscopies, *Thin Solid Films* **582**, 166 (2015).
- [48] M. J. Caldas, A. Fazzio, and A. Zunger, A universal trend in the binding energies of deep impurities in semiconductors, *Appl. Phys. Lett.* **45**, 671 (1984).
- [49] J. M. Langer and H. Heinrich, Deep-Level Impurities: A Possible Guide to Prediction of Band-Edge Discontinuities in Semiconductor Heterojunctions, *Phys. Rev. Lett.* **55**, 1414 (1985).
- [50] M. Turcu, I. M. Kötschau, and U. Rau, Composition dependence of defect energies and band alignments in the $\text{Cu}(\text{In}_{1-x}\text{Ga}_x)(\text{Se}_{1-y}\text{S}_y)_2$ alloy system, *J. Appl. Phys.* **91**, 1391 (2002).